
CORONAL DIAGNOSTIC SPECTROMETER
SOHO

CDS SOFTWARE NOTE No. 54

Version 2

August, 2003



SOHO CDS-GIS Instrument Guide

August 2003

Carl Foley

**Solar and Stellar Physics Group,
Mullard Space Science Laboratory
University College London,
Holmbury St Mary, Dorking,
Surrey, RH5 6NT, UK**

carl.foley@mssl.ucl.ac.uk

Revision list

Version 1, 19 May 1999

Original

Version 2, August 2003

Updated information with regards to LTGD and burn in.

Expanded information on fixed patterning

Included results of ISSI wavelength Calibration.

Included information with regards to the loss and recovery of detector 2.

Included information about the revised field of view of GIS due to the diagnosis of the slit anomaly.

Table of contents

| | |
|--|----|
| 1. Introduction | 4 |
| 2. The GIS Detector System..... | 5 |
| 3. Calibrating GIS Data..... | 6 |
| 3.1 GIS Wavelength Calibration..... | 8 |
| 3.2 Ghosting..... | 8 |
| 3.3 Other corrections and instrument characteristic..... | 7 |
| 3.3.1 Deadtime..... | 11 |
| 3.3.2 Fixed Patterning..... | 11 |
| 3.3.3 Line widths and profiles..... | 13 |
| 3.3.4 Edge effects..... | 14 |
| 3.3.5 GIS Detector 2 – Loss and re-commissioning..... | 15 |
| 3.3.6 Slit Mechanism Anomaly..... | 15 |
| 3.4 GIS Intensity Calibration..... | 15 |
| 3.5 Corrections for Localized Sensitivity Changes..... | 16 |
| 3.5.1 Count-rate gain depression (CRGD)..... | 16 |
| 3.5.2 Long-term gain depression (LTGD)..... | 16 |
| References..... | 19 |

1 Introduction

The SoHO Coronal Diagnostic Spectrometer (CDS) (Harrison et al, 1995) is designed to measure plasma characteristics with spatial, temporal and spectral resolutions and ranges appropriate to study the structure and evolution of the solar atmosphere. It determines this information through the study of emission line characteristics in the extreme ultra-violet (EUV). The performance requirements of the CDS included the need to observe emission lines between 150 and 800 Å, so as to cover ions formed between 10^4 and a few $\times 10^6$ K. This, and the other scientific requirements of CDS, cannot be achieved by a single instrument. Consequently, the CDS is a double spectrometer having the wide wavelength range of a grazing incidence device plus the stigmatic imaging performance of a normal incidence instrument. The CDS uses a grazing incidence Wolter type II telescope to simultaneously feed a normal incidence spectrometer (NIS) and a grazing incidence spectrometer (GIS) through a common slit. This document describes the performance of the GIS, and the origins of the corrections contained in the distributed analysis software.

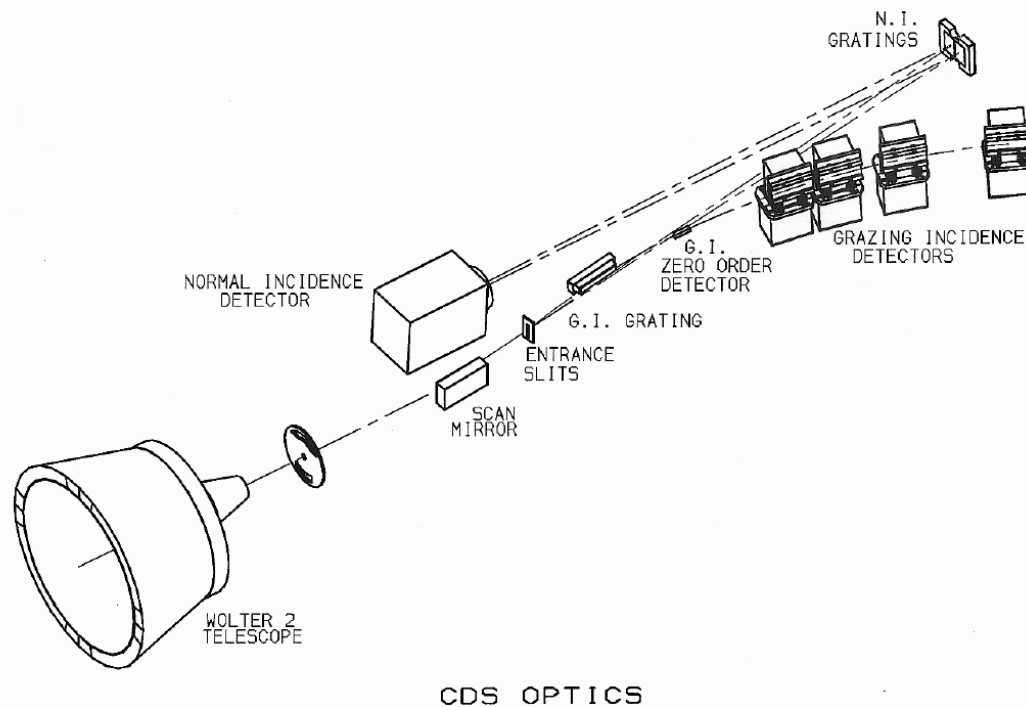


Figure 1: The CDS optical layout. The overall dimensions of CDS are 1.7 m by 0.50 m by 0.46 m. The distance from the entrance aperture to the entrance slits is 0.83 m and from the slits to the normal-incidence grating is 0.74 m.

The GIS instrument (see figure 1), comprises a spherical grating set at grazing incidence, with four micro-channel plate detector systems placed around a Rowland circle. Since the resulting GIS spectra are astigmatic, the instrument builds up images by forming a raster

through incremental movements of a pin-hole slit and scan mirror. The field of view of the instrument is 4x4 arc minutes. Although the prime goal of the CDS is the measurement of line intensities, information on modest to high speed flows have and can be determined, particular with GIS-4.

2 The GIS detector system

Because of the astigmatic nature of the GIS, its detectors only require a one dimension (1-D) capability. The four GIS detector systems are identical (a schematic for one is illustrated in Figure 2), each consisting of a micro-channel plate (MCP) stack in front of a Spiral Anode (SPAN) positional readout (Lapington et al, 1992; Breeveld and Thomas, 1992; Breeveld, 1996) The Z-stack of three MCPs act as a photo-multiplier with each EUV photon producing $\sim 4 \times 10^7$ electrons - the number of electrons produced by an event (the gain) is a function of the bias voltage across the MCP stack. The SPAN readout is illuminated by the electron cloud and accurately determines its position.

The SPAN readout was developed to provide optimal position resolution at a time when space-qualified, fast Analogue to Digital Converters (ADCs) had a maximum resolution of 8-bits. The readout anode consists of a 63x30x3 mm piece of fused silica which is coated with a 2-3 μ m layer of aluminum; a pattern is formed on this using an infra-red laser to create insulating gaps between the electrodes. The anode is divided into a number of identical pitches which are parallel to the dispersion axis of the spectrometer. Each pitch contains the elements of three electrodes (x, y and z) whose areas have the form of damped sine waves; at any position along the anode, the ratio of the fractional charge collected on each electrode is unique. The design of the readout is tuned to the spatial distribution of the electron cloud that emerges from the MCP. The width of the pitch is small with respect to the width of the charge cloud distribution, ensuring that the measured charge is not dependent on the event position in the direction perpendicular to the pitches.

The charge collected on each electrode (Q_x , Q_y and Q_z) is measured using a sample and hold circuit and the values are converted to digital outputs with 8-bit ADCs. The total charge on the three electrodes ($Q_t = Q_x + Q_y + Q_z$) is used as a reference input to the ADC to normalize the different sized electron clouds.

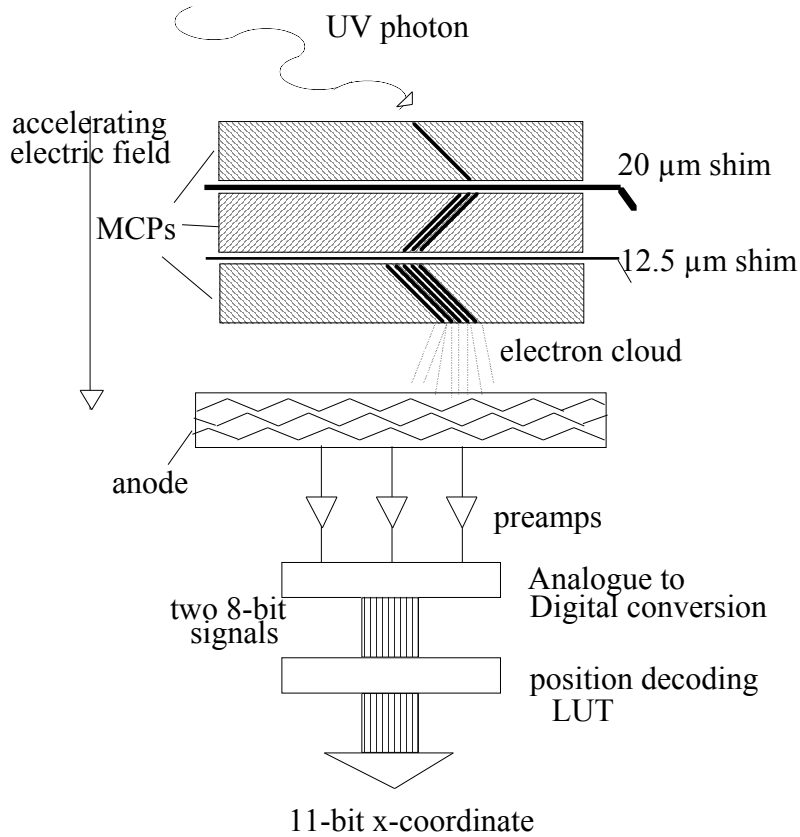


Figure 2: Schematic diagram of a GIS detector showing the path through a detector from a single photon to a single co-ordinate in the output image.

The x and y outputs of the ADCs therefore have the values $x=Q_x/Q_t$ and $y=Q_y/Q_t$. These are used as coordinates in a look-up table (LUT) to determine the actual position of the incoming photon. The look-up table is assembled by the instrument using an algorithm that calculates the table entries from parameters uplinked from the ground in a GIS setup block (or GSET). The GSET parameters are adjusted for each type of observation, high voltage setting and slit size. They are determined by examining the GIS RAW dumps which contain the x and y positions of each photon as output by the ADCs, i.e. the un-encoded lookup values. The GIS detector system is susceptible to a number of instrumental effects.

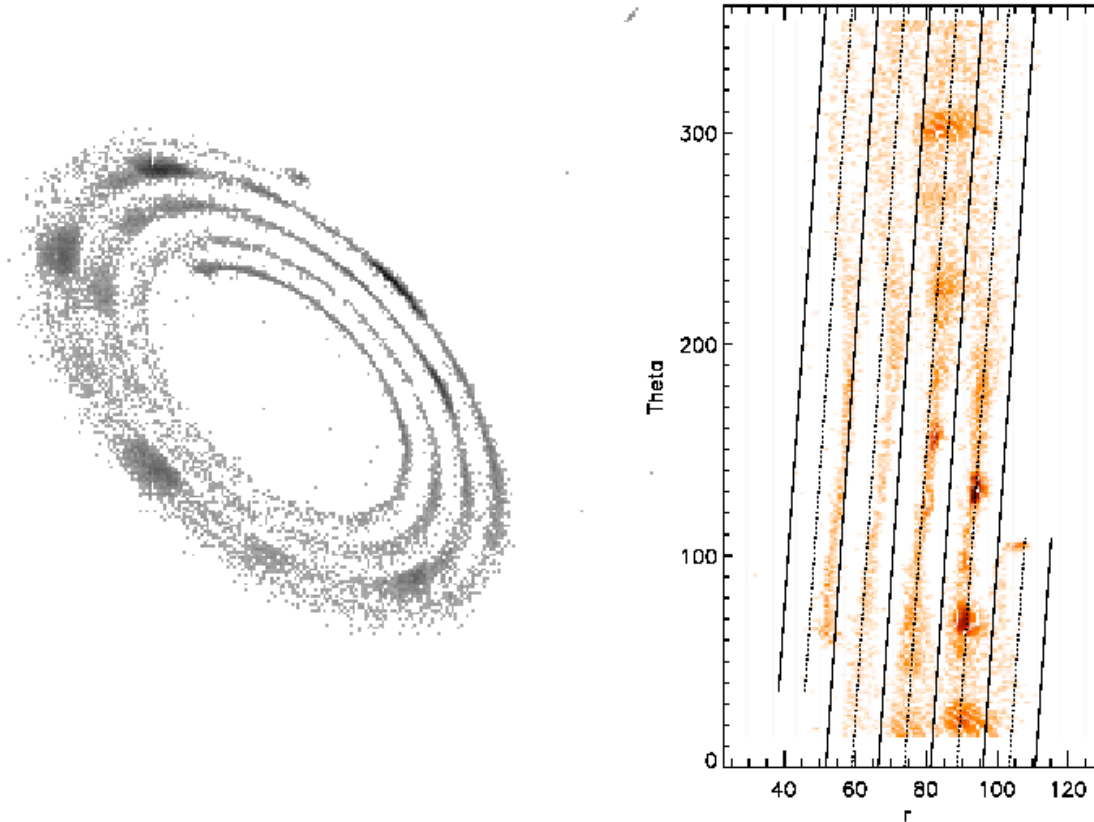


Figure 3: The ADC outputs x and y plotted in a) Cartesian coordinates (top-left) and b) r - θ coordinates (top-right). Each cycle of the sine wave in the SPAN readout pattern is represented by a turn in the spiral in (a) or an arm in (b). The innermost end of the spiral in (a) is equivalent to the bottom of the leftmost strip in (b).

Some of these are easier to understand if the GIS RAW dumps are plotted in different ways. The SPAN electrodes take the form of phased, decaying sine waves. When the digitized x and y values output by the ADCs are plotted in Cartesian coordinates they form a spiral (see Figure 3 a) - the position along the detector is determined by the distance along the spiral. When they are plotted in r - θ space, the values form a series of diagonal stripes, one for each cycle of the sine wave of the SPAN readout (see Figure 3b) – here, “ r ” is the distance from the centre of the spiral, and “ θ ” the angle around the spiral. The GSET is adjusted to try to provide the best fit to the stripes on the r - θ plot. Inadequacies in the fit caused by distortions in the spiral, combined with errors in the values of x and y (caused by offsets in the analogue electronics), mean that some events are incorrectly encoded to the adjacent arm of the spiral (see Ghosting). The discrete nature of the entries in the look-up table, which try to represent the continuously varying function of the Spiral, leads to a digitization noise (see Fixed Patterning).

3 Calibrating GIS Data

Reading and calibrating the GIS data is performed using the Solarsoft IDL[®] library which is maintained and distributed at Lockheed Martin (<http://www.lmsal.com/solarsoft>) and the Solar UK research Facility at MSSL (<http://surfwww.mssl.ucl.ac.uk/solarsoft>), where full instructions and support for the installation and maintenance of the software is available. The analysis of the GIS data is simplified by the use of the GIS analysis routines which form part of the Solarsoft library particularly (in order of use) – **GIS_LTGD_CALIB**, **GHOST_BUSTER**, **GIS_SMOOTH**, and **GIS_CALIB**. These routines enable users to quickly and accurately obtain the intensity and wavelength calibrated data. The user guide describes how these corrections can be used. In this guide we describe the origin of these calibrations and any issues relating to instrument calibration and instrument effects that must be considered when analysing the GIS data.

3.1 GIS Wavelength Calibration

The wavelength calibration of the GIS was determined by pre-launch calibrations (Bromage et al., 1996; Lang et al., 1999) and has been confirmed in flight. The calibration is automatically applied to GIS spectra as the data are read from a FITS file into a quick-look data structure (QLDS) using **readcdsfits**. The wavelength calibration across the individual GIS detectors can be described by a combination of three functions, a slow quadratic term introduced by the electronic encoding, a complex almost linear term from the dispersion from the grating, and a cyclic term because the detectors are not curved with the Rowland circle. This latter function is a third order term and is not normally used. As described earlier, the electronic position encoding uses a lookup table (LUT) to determine the event position from the charge measured on the anode electrodes. Two parameters in the GSET used to construct the LUT affect the shape of the wavelength dispersion for the detector; the parameters do not affect the wavelength coverage of the channel. These optical and electronic effects are folded into the wavelength calibrations that have been prepared for each GSET.

3.2 Ghosting

The performance of the spiral anode readout used for the GIS detectors can be affected by an ambiguity in the position of incoming photons. This occurs at certain phases of the sine wave pattern of the SPAN readout and translates into “ghost” in some regions of the resulting spectrum.

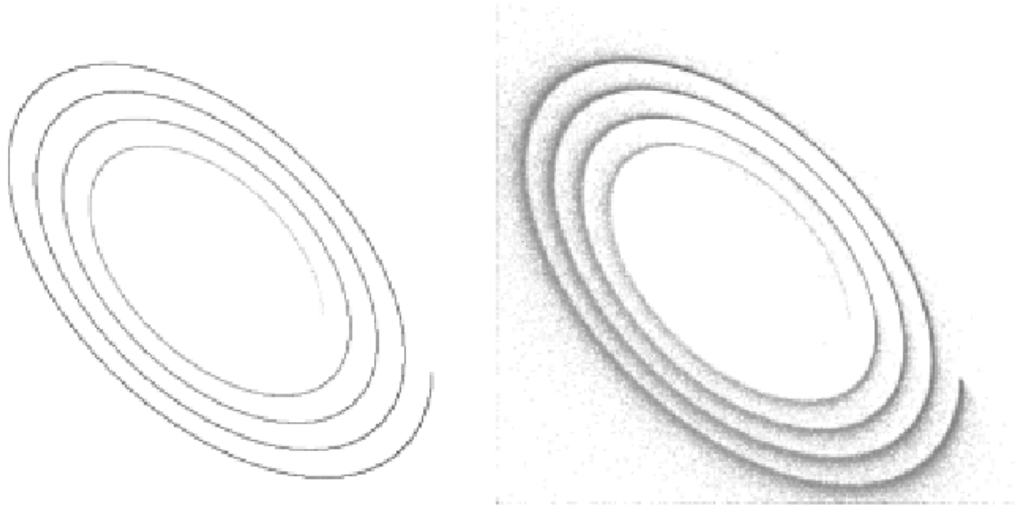


Figure 4: This plot shows a simulation of ghosting: an ideal, synthetic spiral (left), and its appearance when offsets are introduced into the analogue electronics (right), Compare the right-hand image with the spiral in figure 3 in the simulation, the ratio of the offsets for x-y and z was 2:2:1

The counts in the ghosts must be added to the original lines before an intensity calibration can be performed. The performance requirements specified for the GIS included the ability to handle a high count rate - up to 20000 counts per second per detector. The analogue to digital converters and other analogue components were selected to meet this requirement within the power constraints of the instrument. However, when the flight model instrument was integrated, the processing electronics were found to be affected by electronic noise. One consequence is the appearance of small offsets in the analogue electronics that produce increased errors in the x and y outputs of the analogue to digital converters - this translates into a positional uncertainty when the event pulse heights are small. The effects have been simulated and the results of the model agree well with the observed spiral, see Figure 4 - ghosts occur where the width of the spiral is broadened by the effects of the offsets. The spiral arms overlap each other in these regions of the detector and this introduces a leaking of position data in the resulting spectrum. This can also be seen in the three plots in figure 5 which were generated from an observation of the quiet Sun. In this Figure the darker regions in the spiral are the spectral lines, when plotted in r-theta space, some of these are seen to spread, or ghost into adjacent arms of the spiral. The lower plot shows the spiral unraveled and then summed to produce a spectrum. Ghosts can be seen as features entering from the top or bottom of the greyscale strip where they have spread from an adjacent arm of the spiral, the direction of entry depends on whether the line has ghosted from the blue or red side. It can be seen that the ambiguity (or ghosting) in spectral data does not occur over the whole spectral range, and that where ghosting occurs it is conferred to specific locations in adjacent spiral arms. This allows the GIS analysis software – **ghost_buster** and associated routines, to characterise the ghosts as detailed in the User Guide. When correcting for ghosts, the counts in the ghosts must be added to the counts at the original location to produce the observed line intensity which can then be corrected for instrumental effects and

calibrated. This is in most cases routine, since ghosting occurs in predefined locations and most often in places where no other lines form. In this case the data are automatically corrected using the **ghost_buster** routine. Currently, about 70% of the spectrum is recovered using the **ghost_buster** non-interactively. For the regions where lines ghost directly on top of other lines, manual investigation and correction (see CDS-GIS analysis guide for more information). Work is in progress to allow these regions to also be recovered automatically.

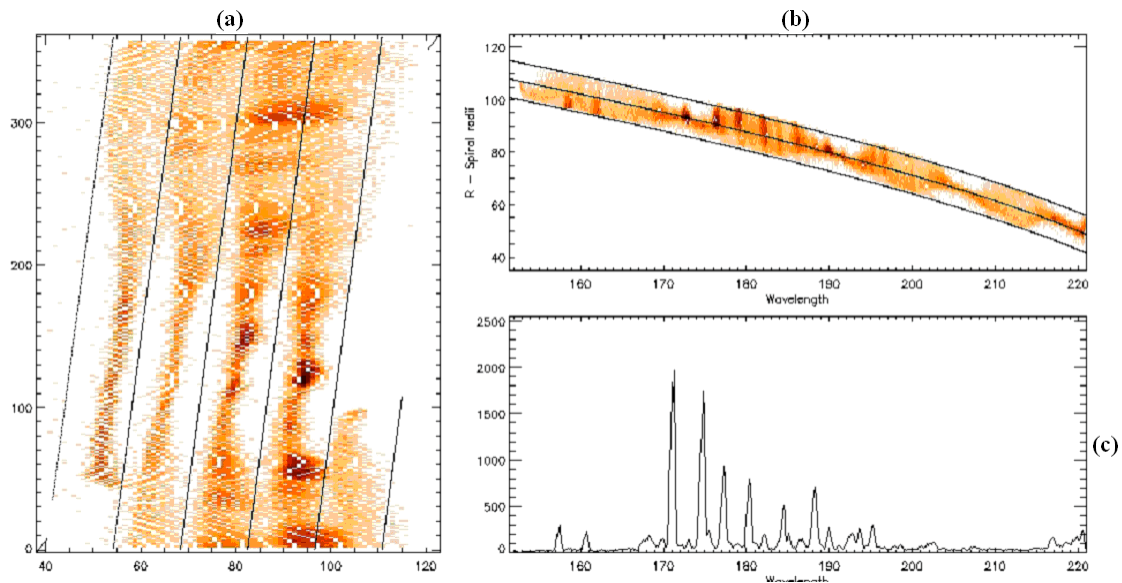


Figure 5: A GIS RAW dump plotted in three different ways: a) unwound in r-theta coordinates (left), b) as a strip that follows the spiral (top-right), and (c) - a vertical summation of this produces the GIS spectrum. The innermost end of the spiral in (a) is equivalent to the long wavelength (rightmost) end of the spectrum in (b and c) – i.e. the wavelength decreases as you move outwards around the spiral. The ghosts can be seen in (a) as regions where the emission lines are split by unwinding the spiral as per the LUT. In this case ghosting only occurs in the 174-185 nm range, but is easily corrected for using **ghost_buster** non-interactively.

3.3 Other corrections and instrument characteristics

3.3.1 Dead-time

In common with most detector systems of this type, there are dead-times associated with the processing electronics. They affect the data at relatively high count rates and only limit the GIS throughput above 10^5 counts per second: i) An extending dead-time for each detector related to the time taken for analogue electronics to process an event and settle to their nominal level. ii) A non-extending dead-time, affecting all detectors, related to the multiplexing of the position data produced by the four detector systems into one stream. This is sometimes called quiz-show dead-time. iii) A non-extending dead-time, affecting all detectors, related to the FIFO buffer. This buffer evens out the flow of data into the CDS CDHS unit. These dead times are corrected for using the routine **gis_calib**.

3.3.2 Fixed patterning

Position encoding of the GIS detector is implemented using a look-up table (LUT) - the coordinates used to determine the converted position from the LUT are provided by the digitized charge from the x and y electrodes. An inadequate resolution in the LUT has resulted in fixed patterning, where adjacent pixels share varying amounts of the incoming counts (Breeveld et al., 1996). This is common and arises with many position-sensitive detectors where the measured quantities, in this case the collected charge, are digitised before being divided (*Geesman et al.*, 1991). This gives an excess of events in some bins with a corresponding decrease in others. Although the positions of the photons are shifted, the total number of counts is conserved and line intensities are unaffected. To overcome this, you can either smooth the data or reduce the sampling. The routine **GIS_SMOOTH** uses a Hanning function to smooth the data. The use of this routine preserves the total events in the lines with a relatively small increase in the width of the line.

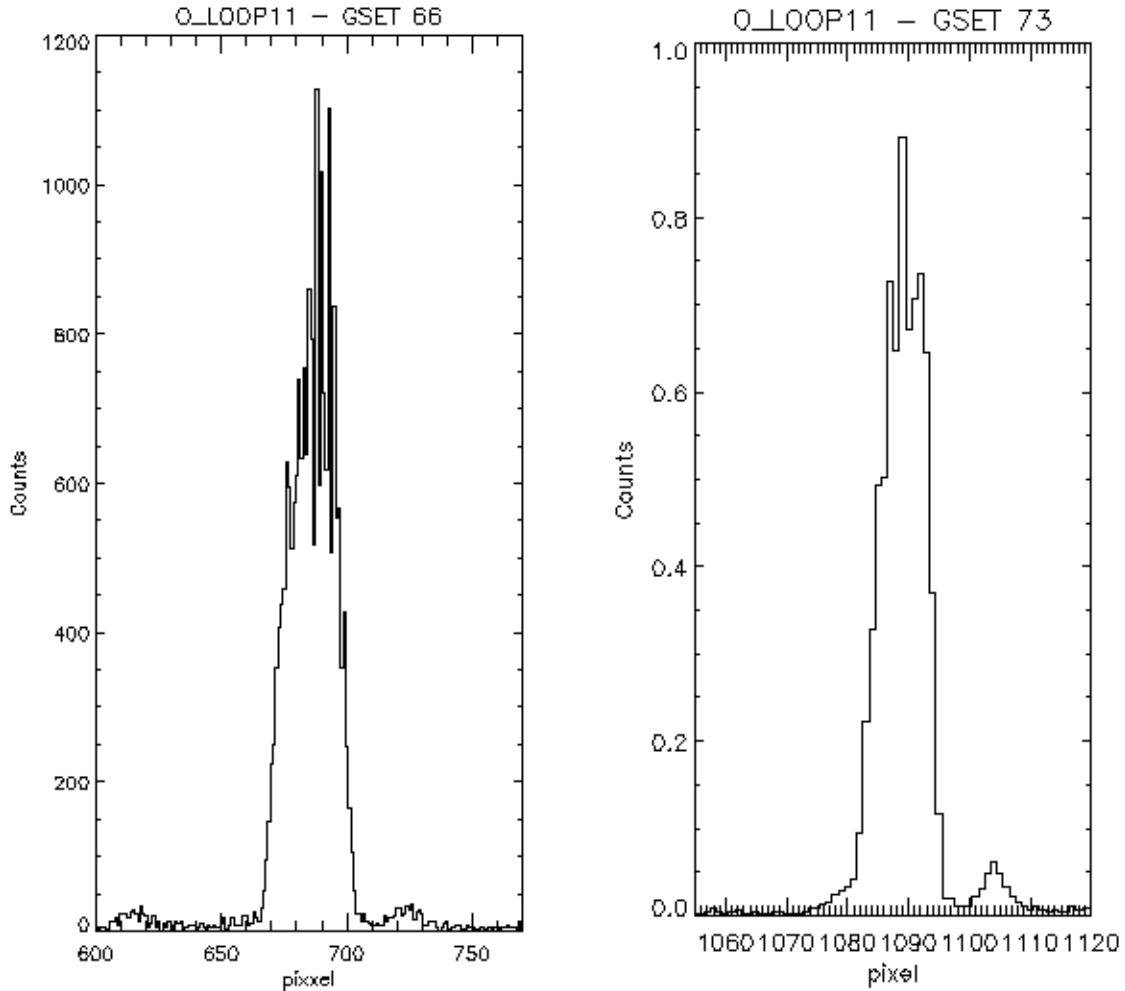


Figure 6: An example of the fixed patterning seen in the GIS for the Fe XIV 284 _ line (left). The fixed patterning can be greatly reduced by rebinning, through the use of novel GSET LUT settings.(right)

The affects of fixed patterning can be seen in the left hand panel of figure 6 as a salt and pepper noise over the spectra. Fixed patterning is also visible on the r-theta plot in figure 3 and 5, as a “wood-grain” pattern superimposed on the spiral arms. Before the GIS data are analysed, a simple smoothing algorithm is applied to reduce the fixed patterning. It is possible to produce a GSET to reduce the sampling (increase the pixel size). An example of this is illustrated in the right hand panel of figure 6. This removes the effects of fixed patterning, and improves the statistical quality of the data. However, the wavelength and intensity calibration need to be done manually since the calibration software needs to be modified to handle data produced by non standard GSETs.

3.3.3 Line widths and profiles

The GIS line widths are larger than expected and their shapes are anomalous. The line profiles cannot be fitted with single Gaussians. Their unusual nature was reported by Bromage et al., 1996 in their analysis of data from ground calibrations. Typical widths for lines observed by the GIS with different slits are shown in figure 7 - this also shows the expected line widths (from the "Blue Book"), and the "stim pulse" line widths. It is unclear whether the cause of the anomalous profiles is an optical or detector effect.

The detector processing electronics can be tested using stim pulses that are applied to pads on the back face of the anode plate, and capacitive couple to the anode electrodes. The stims are normally switched off but can be commanded ON from the ground. That the stim pulses form a narrow profile implies that the anomalous width of the spectral lines is not caused by the processing electronics but must arise before the SPAN readout system. This implies an effect either related to the MCP, or within the optics of the spectrometer. Although, the lines are not ideal it is still possible to take moments and make studies of plasma dynamics.

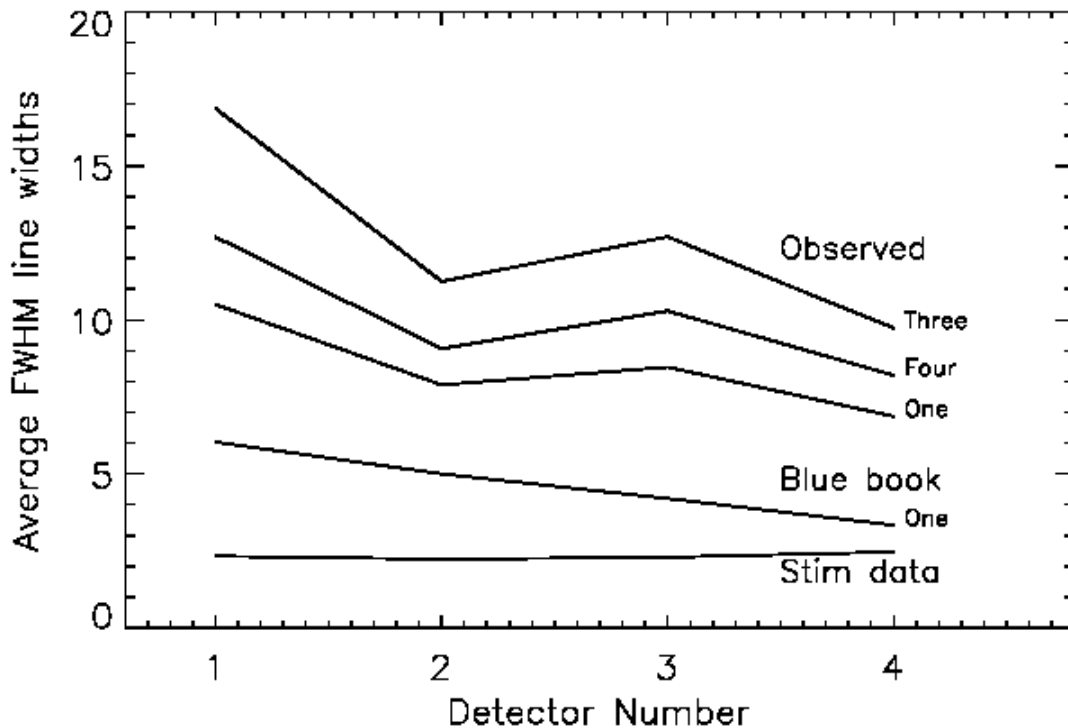


Figure 7: A comparison of line widths of the GIS (in pixels). The bottom line is the width of the stim, the next line is the expected "Blue Book" width for slit one, and the top three curves the observed widths for slits one (2x2 arcsec), three (8x50 arcsec), and four (2x240 arcsec).

Since the counts are just redistributed in the vicinity of the line and not lost, the primary objective of the GIS system - to measure line intensities - is not affected. The NIS line widths are also slightly larger than expected and it has been suggested that some of the

difference in both instruments might be due to the fact that the preflight measurements were made using a narrow-beam source. There are currently no corrections for line shapes within the software, with the exception of the gain depression corrections described below.

3.3.4 Edge Effects

At the ends of the GIS detectors, particularly the long wavelength end, the background level is seen to increase. This is partly due to a compression in the wavelength scale in the end regions of the detector where it deviates from the assumed parabolic shape. Another cause includes secondary emission from the spectrometer structure. In the GIS-3 and GIS-4 channels, an edge effect that is due to real He continuum is visible. This is seen only in observations made on the solar disk. In the case of GIS-2 there are very strong lines at the beginning of detector which should not be confused with edge effects. Preliminary corrections for the non solar sources are now included in **gis_calib**. These have relatively large errors associated with them (which are passed into the output structure). These will reduce as we acquire more observations to check the corrections.

3.3.5 GIS Detector 2 – Loss and re-commissioning

During the spring of 1999 very high and modulating background levels were observed in detector 2. The reason for this was unclear and the detector was turned off on the 26th April 1999. It was believed that this was most probably due to contamination of the MCP's from material out-gassing from the electronics. The level of this background was monitored intermittently until the detector appeared nominal again. The detector was recommissioned on the 20th June 2001.

3.3.6 Slit Mechanism Anomaly

During the middle of 2001, an anomaly was identified in the positional data reported for observations made with the GIS. Investigations revealed that the GIS was sticking in one particular location (+40 arc seconds). Since, the slit mechanism is central to CDS and not only controls the rastering for the GIS but also changing the slit for all CDS observations, the use of it for GIS rastering was stopped, whilst the reason was diagnosed. It appears likely that the anomaly was associated with the positional encoder and is not mechanical in nature. Given the importance of the slit mechanism to the operation of CDS, and the fact that most GIS observations don't make use of the full range of motion available, the planning software has been modified so that the effective field of view of GIS is 4x2.5 arcmin.

3.4 GIS Intensity Calibration

The intensity calibration for the GIS was determined before launch in tests at RAL (Bromage, et al., 1996, Lang et al., 1999), and confirmed in-flight using a DEM technique across all four GIS detectors (Landi et al., 1998). The absolute and relative calibration was obtained and is maintained by making a number of cross calibration observations in collaboration with the other instruments on SoHO, as well as periodic rocket flights such as the SERTS series in 1996, 1997 and the Wood-Hassler rocket in 1997. These data were used during two “radiometric intercalibration of SOHO” workshops, which were held at the International Space Science Institute (ISSI) in Bern during 2001, to determine the intensity calibration. The result of these meetings was that the sensitivity of the GIS and CDS as a whole was found to be 2.6 ± 0.9 greater than the laboratory calibration (see Figure 8), before the recovery of SOHO, and 2.1 ± 0.7 after the SOHO recovery. Since the two factors agree, a single factor of 2.6 ± 0.9 is applied in the software. This factor compares well with a comparison of common lines in NIS and GIS in which Del Zanna et al., found a factor of 2.2. These intensity calibrations are applied to the data using the analysis routine **gis_calib** (see the User Guide). The data acquired around the time of the SOHO recovery is being investigated further for evidence of changes in the sensitivity of CDS.

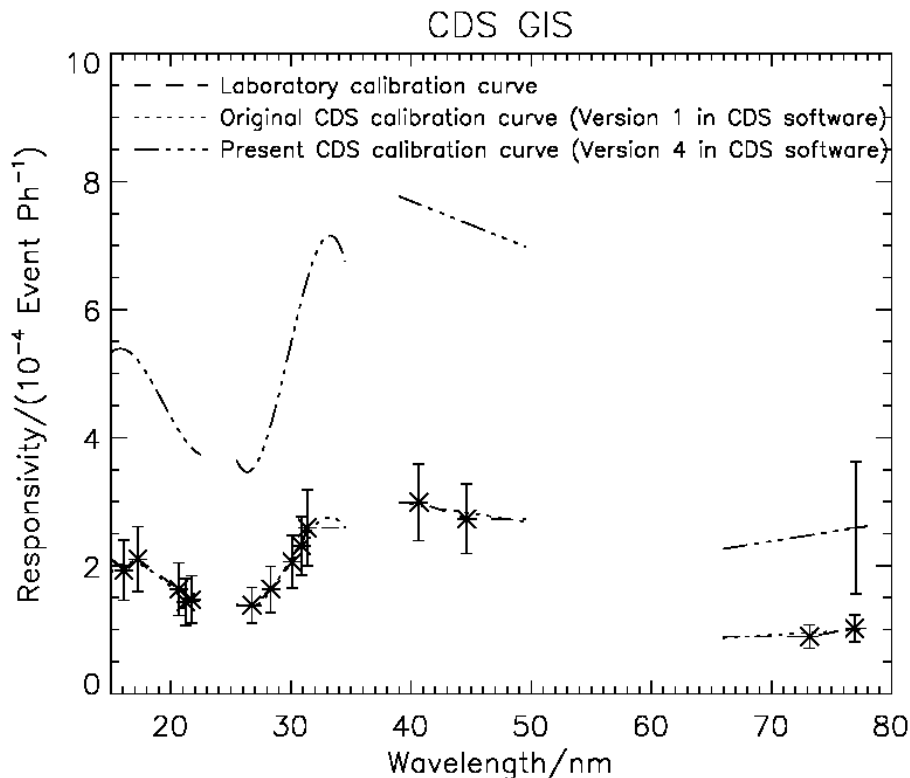


Figure 8: The CDS GIS response as a function of wavelength. The version numbers are chosen to be consistent with those used for the NIS.

3.5 Corrections for Localized Sensitivity Changes

The sensitivity of a detector system evolves in time, depending on how much the detectors and instrument as a whole evolves in time. These changes are usually attributed to changes such as aging (contamination, outgassing) as well as reduction and loss in sensitivity related to accumulated dose. In the case of micro-channel plates as used in CDS, localized high count-rates affect the sensitivity greatly and must be taken into account. These are outlined below and discussed in detail in Breeveld (1996) and Foley et al., 2003.

3.5.1 Count-rate gain depression (CRGD)

A micro-channel plate (MCP) works by creating an avalanche of electrons when a photon enters a channel in the MCP. There is a finite time (between 3 and 100 ms) required to recharge the channels after a pulse of electrons has been released and the gain that can be sustained by the channel plate is inevitably reduced as the photon count-rate increases. The count-rate per pore is the most important parameter - a high count-rate across the whole plate does not induce gain depression (although electronic deadtimes may affect the overall throughput). In the GIS detectors, this type of count-rate gain depression (CRGD) is observed in the regions of intense spectral lines occasionally. The effect is corrected for in the analysis software (**gis_calib**) up to a predetermined count-rate (65 counts/sec) in a pixel - beyond that the region of the detector is marked as uncalibrated.

3.5.2 Long-term gain depression (LTGD)

In regions close to excessively bright lines in the GIS suffers an accumulating and long-term loss in sensitivity. This is due to a reduced efficiency in the production of secondary electrons from the channel walls, due to the creation of electron traps within the lattice of the MCP material. The degradation depends on the total charge extracted, not the rate of extraction or gain. This loss in gain has been observed since launch for the He II at 304 Å in detector 2, but hadn't thought to have been a problem for the other less bright lines since the High voltages of the detectors are maintained with fully saturated FWHM.

The overall gain of the GIS detector system is maintained by adjusting the detector high voltage settings. The detectors are usually run so that the pulse height distribution is fully saturated - the FWHM of the distribution being between 80 and 120%. If the detectors are uniformly illuminated, a gradual increase of the HV's to maintain a fully saturated FWHM, would result in no loss in gain of the detectors. However, since the detectors are not uniformly illuminated any change in the HV's will result in a partial restoration of gain in very exposed regions at the expense of a loss of linearity across the detector.

The GIS detectors have filaments built into to monitor the degree of LTGD them. These filaments produce a cloud of electrons which simulate the effect of incident photons to estimate the flat field. However, because the electron clouds are relatively inhomogeneous, and they illuminate the whole of the detectors (only 1/50th of the detectors are usually illuminated by the GIS prime slits.) the actual degree of the LTGD, has proved difficult to track reliably. This has until recently made it difficult to accurately correct the gain depression across the detectors.

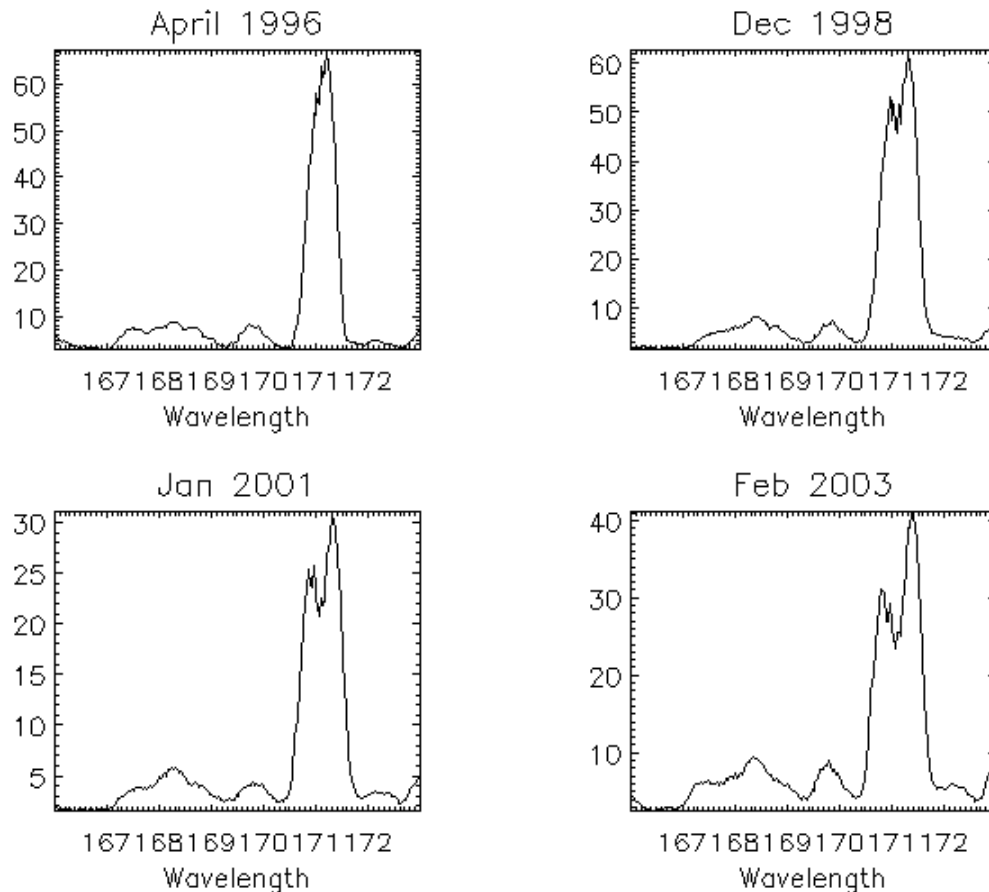


Figure 9: Typical Grazing incidence micro-channel plate (GIMCP) observations of the Fe IX 171 _ line over the mission. The evidence of LTGD is clearly apparent with the dimple effect at the line center.

The effect of gain depression, is now easily recognizable in the data (see Figure 9). This is seen in the apparent increased widths of the emission lines and the “dimpling” of lines. This dimpling is caused by a preferential loss of sensitivity towards the center of the line. This is illustrated in Figure 9, for the Fe IX 171 _ line, the brightest line in GIS 1. Modeling the increasing width and making comparisons with the filament data suggests that the Fe IX 171 line has reduced in sensitivity by approximately 70% (During July 2003, we have increased the HV’s for detector 1 to compensate for much of this loss). These measurements and comparisons with other bright lines have been used to estimate the LTGD across all the detectors (see Foley et al., 2003). This correction is based on an

estimate of the total accumulated charge extracted from the detectors, and is applied to the data using the standard analysis software (**gis_calib_itgd**, which is called by **gis_calib**). The uncertainty in this correction remains fairly high at around the 20% level. However, new engineering studies are being created which will enable the HV to be changed during observations, allowing the production of gain curves for each observed line. This will allow the accuracy of the correction to be assessed so that the correction may be refined and the associated uncertainty reduced.

References

- Bromage, B.J.I., Breeveld, A.A., Kent, B.J., Pike, C.D., and Harrison, R.A., "Report on the pre_launch Calibration of CDS", UCLan Report CFA /96/06
- Breeveld, A.A., "Ultraviolet Detectors for Solar Observations on the SOHO Space-Craft" University of London Ph.D. Thesis, 1996.
- Breeveld, A.A. and Thomas, P.D., "The Grazing Incidence Detectors for the SOHO Coronal Diagnostic Spectrometer", Proceedings of an ESA Symposium on Photon Detectors for Space Instrumentation.
- Breeveld, A.A., Edgar, M.L., Lapington, J.S. and Smith, A., 1992, "The effects of charge cloud size and digitization on the SPAN anode" in "EUV, X-ray, and gamma-ray instrumentation for astronomy III", Proceedings of the Meeting, San Diego, CA, July 22-24, 1992, 315-326.
- Harrison, R.A. et al., 1995, "The Coronal Diagnostic Spectrometer for the Solar and Heliospheric Observatory", Sol. Phys., 162, 233.
- Harrison, R.A. et al., 1995, "The Coronal Diagnostic Spectrometer for the Solar and Heliospheric Observatory", the "BLUE" book, RAL Report SC-CDS-RAL-SN-95-001.
- Landi, E., Del Zanna, G., Breeveld, E.R., Landini, M., Bromage, B.J.I., Pike, C.D., 1999, "Relative intensity calibration of CDS-GIS detectors on SOHO using a plasma diagnostic technique", Astronomy and Astrophysics Supplement, v135, p 171-185.
- Lang, J., Kent, B.J., Breeveld, A.A., Breeveld, E.R., Bromage, B.J.I., Hollandt, J., Payne, J., Pike, C.D., and Thompson, W.T., 1999, "The Laboratory Calibration of the SOHO Coronal Diagnostic Spectrometer", RAL Report RAL-TR-1999-036.
- Lang, J.; Thompson, W. T.; Pike, C. D.; Kent, B. J.; Foley, C. R., 2002, "The Radiometric Calibration of the Coronal Diagnostic Spectrometer", The Radiometric Calibration of SOHO, ISSI Scientific Report SR-002. Edited by A. Pauluhn, M.C.E. Huber and R. von Steiger. ESA Publications Division, Noordwijk, The Netherlands, 2002., p.105
- Lapington, J.S., Breeveld, A.A., Edgar, M.L. and Smith, A., 1992, "Performance characteristics of SPAN position readout systems" in "EUV, X-ray, and gamma-ray instrumentation for astronomy III", Proceedings of the Meeting, San Diego, CA, July 22-24, 1992, 303-314.
- Lang, J.; Thompson, W. T.; Pike, C. D.; Kent, B. J.; Foley, C. R., "The Radiometric Calibration of the Coronal Diagnostic Spectrometer" in "The Radiometric Calibration of SOHO, ISSI Scientific Report, Pauluhn, A., Huber M.C.E., von Steiger, R. eds
- Foley, C.R., Culhane, J.L., Lang, J., "Ageing of the Grazing Incidence Spectrometer on SOHO", submitted to Journal of Optics A: Pure and Applied Optics.
- Del Zanna, G., Bromage, B.J.I., Landi, E., and Landini, M., "Solar EUV spectroscopic observations with SOHO/CDS I. An in-flight calibration study", Astron. Astrophys. 379, 708-734, 2001